

Determining bathymetry of shallow and ephemeral desert lakes using satellite imagery and altimetry

M. Armon¹, E. Dente^{1,2,3}, Y. Shmilovitz^{1,2}, A. Mushkin², T. J. Cohen⁴, E. Morin¹, and Y. Enzel¹

¹The Fredy and Nadine Herrmann Institute of Earth Sciences, the Hebrew University of Jerusalem, Israel.

²The Geological Survey of Israel, Israel.

³Shamir Research Institute, University of Haifa, Israel.

⁴School of Earth and Environmental Sciences, University of Wollongong, Australia.

Corresponding author: Moshe Armon (moshe.armon@mail.huji.ac.il)

Key Points:

- A new methodology to produce bathymetry maps of shallow desert lakes was developed, based on globally available datasets
- The methodology enables mapping the bathymetry of lakes with sub-basins or partially flooded lakes; both major limitations of other methods
- The derived bathymetry error is ~30 cm, rather than ~2.5 m for other globally available data

1 **Abstract**

2 Water volume estimates of shallow desert lakes are the basis for water balance calculations,
3 important both for water resource management and paleohydrology/climatology. Water volumes
4 are typically inferred from bathymetry mapping; however, being shallow, ephemeral and remote,
5 bathymetric surveys are scarce in such lakes. We propose a new, remote-sensing based, method
6 to derive the bathymetry of such lakes using the relation between water occurrence, during >30-
7 yr of optical satellite data, and accurate elevation measurements from the new Ice, Cloud, and
8 Land Elevation Satellite-2 (ICESat-2). We demonstrate our method at three locations where we
9 map bathymetries with ~0.3 m error. This method complements other remotely sensed,
10 bathymetry-mapping methods as it can be applied to: (a) complex lake systems with sub-basins,
11 (b) remote lakes with no in-situ records, and (c) flooded lakes. The proposed method can be
12 easily implemented in other shallow lakes as it builds on publically accessible global data sets.

13 **Plain Language Summary**

14 Lakes in desert environments are often remote, shallow, and only get filled once in a long while.
15 They are an important water resource, and could be used to decipher past environmental
16 conditions. However, detailed maps of lake-floor terrain, which are required to effectively study
17 these lakes are typically not available. The deepest parts of the lakes are filled with water more
18 frequently than their shallow margins. Thus, we suggest here to relate water occurrence in those
19 lakes with accurate satellite-based elevation measurements, to obtain a valuable lake-floor terrain
20 map. We demonstrate the usefulness of our method by comparing results with other globally
21 available data. Previous methods struggle with complex-terrain lakes or lakes that are partially
22 flooded during their survey; while our method yields high-resolution accurate maps even in such
23 lakes.

24 **1 Introduction**

25 A major characteristic of drylands is endoreism, internal drainage (de Martonne, 1927). The lower and usually drier
26 parts of these drylands are often occupied by ephemeral or seasonal shallow desert lakes (Nicholson, 2011).
27 Thousands of such lakes exist globally with the largest being Lake Eyre (Australia, alias Kati Thanda; surface area
28 of >9000 km² when full). Such lakes are significant for opportunistic species that have no other water resources
29 (e.g., D'Odorico and Porporato, 2006; Noy-Meir, 1973). Mapping of lake floors is key in calculating water balance
30 (e.g., Cohen et al., 2015; Enzel and Wells, 1997), important in water resources management, and in deciphering
31 paleohydrology (e.g., Crétaux et al., 2016; Quade et al., 2018). However, being shallow, dry and remote,
32 bathymetric surveys (e.g., as in Bye et al., 1978) have been scarce in such lakes.

33 A different approach to bathymetry mapping is through remote-sensing (Gao, 2015; Jawak et al., 2015). The Shuttle
34 Radar Topography Mission (SRTM) has provided high resolution (~30m) global digital elevation models (DEMs)
35 that could, in principal, present bathymetry of such desert lakes. Yet, radar altimetry cannot produce accurate DEMs
36 if the area is flooded or where lake floors are exceptionally bright and/or smooth (Berry et al., 2007; Brenner et al.,
37 2007), which are common conditions.

38 To improve lake bathymetry maps, recent studies either integrate remote-sensing with a spatial interpolation of in-
39 situ measurements (Feng et al., 2011; Leon and Cohen, 2012) or combine between optical imaging and radar (e.g.,
40 Sun and Ma, 2019) or laser altimetry (Arsen et al., 2013; Li et al., 2019; Ma et al., 2019). These satellite imaging
41 methods are based on determining isobaths (equal depth lines) of a lake, through snapshots during different lake
42 stages. Then, shorelines in each specific image are assigned a height through accurate elevation measurements; such
43 as laser altimetry. This determines bathymetry only to the depth of the lowest shoreline identified, using a spatial
44 interpolation of a few isobaths. It also overlooks the possible variance in elevation of a specific shoreline, which can
45 be significant in large lakes (Arsen et al., 2013; Feng et al., 2011). Li et al. (2019) suggested using a long-term (410
46 images during >30-yr) water occurrence index, instead of a few specific isobaths, and relating it with measurements
47 from a limited dataset of airborne lidar altimetry. This overcomes shoreline elevation variations and makes spatial

48 interpolation unnecessary. However, they assumed a linear relation between isobath areas, sampled at specific
49 points, and elevation. Applying their methodology to a deep reservoir (Lake Mead; >100m deep) only revealed the
50 bathymetry of the upper part of the lake; the deeper bathymetry was extrapolated with geometrical considerations,
51 calibrated using in-situ data (Li et al., 2019). A further complication arises where water occurrence is not based
52 directly on elevation, primarily where a lake is composed of a few sub-basins, which yields more than one possible
53 relation between water occurrence and elevation. Accordingly, present-day methodologies and freely available
54 datasets cannot provide accurate, high-resolution bathymetry of often-flooded, shallow desert lakes, especially for
55 lakes having more than one sub-basin.

56 Thus, to derive the bathymetry of desert lakes, there is a need for: (a) an efficient and reliable way to recognize the
57 water occurrence at a high resolution, (b) a technique to overcome diverse water occurrences-elevation relations in
58 different sub-basins, (c) a way to derive the bathymetry when lakes are inundated, (d) a robust method to validate
59 the resulted bathymetry. To tackle these challenges, we developed a simple and easily implemented methodology
60 that derives bathymetry of shallow desert lakes. This paper focuses on three desert lakes, ranging in area from
61 $0.2 \times 10^3 \text{ km}^2$ to $6 \times 10^3 \text{ km}^2$. Lake bathymetries are acquired using the relation between globally-available high-
62 resolution (30 m) water occurrence maps, and elevation data from NASA's new Ice, Cloud, and Land Elevation
63 Satellite-2 (ICESat-2).

64 Following is a description of the methodology and its application over Lake Eyre, which consists of a few sub-
65 basins. We show the derivation of a bathymetric map for the lake and validate it versus the global SRTM and the
66 best bathymetric map available for the region (Section 3). Having better results than the SRTM, we set to derive the
67 bathymetry of a remote lake in the Sahara (Sabkhat El-Mellah) that has no other bathymetric map (Section 4) and of
68 Lago Coipasa in the Altiplano for which we separately derive the bathymetry under dry and inundated conditions.

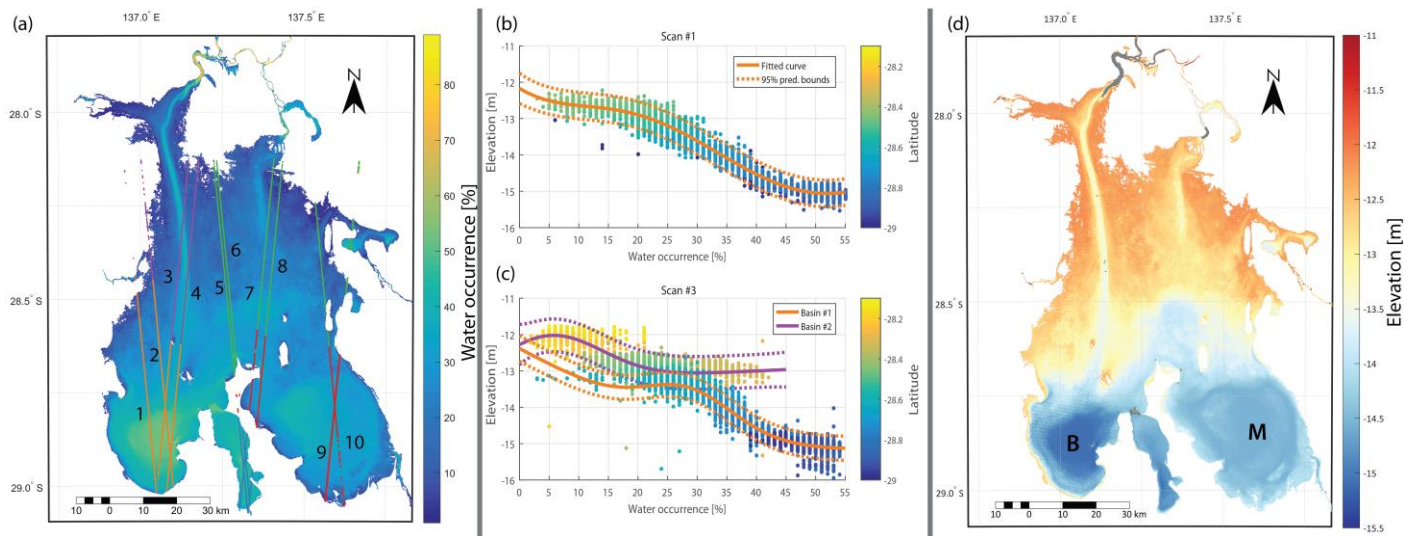
69 **2 Methodology**

70 Desert lakes are often fed by floods with monthly to decadal frequencies. Most of the coarser particles are deposited
71 upstream, and thus, lake floors are mainly covered with fine low-permeability sediments, making evaporation the
72 primary output (Nicholson, 2011). Water occurrence in these lakes is <100% of the time, and often <30%. Thanks to
73 a detailed analysis of 3×10^6 Landsat images by Pekel et al. (2016), the frequency of water occurrence over 30 m
74 pixels between 1984 and 2015 is easily accessible worldwide. Water occurs more often over the deeper parts of the
75 lake, where complete evaporation takes longer, and less often over the higher lake margins. Thus, there should be a
76 straightforward relation between water occurrences (i.e., the relative frequency of water in a pixel) and lake floor
77 elevation over such lakes. This, in turn, allows measuring height over specific locations within the lake, from which
78 we can infer the lake floor elevation.

79 ICESat-2 provides dense and accurate elevation measurements (0.7 m point spacing; accuracy and precision of <5
80 cm and <13 cm, respectively) over land, and even underwater. Thus it yields accurate, narrow height profiles of
81 lakes, since its launch in September 2018, with a 91-day revisiting frequency (Brunt et al., 2019; Markus et al.,
82 2017). Underwater measurements can penetrate up to ~1 Secchi depth (Parrish et al., 2019), i.e. up to a few meters
83 or even a few dozens of meters (Ma et al., 2019), depending on the optical properties of the water.

84 Relying on the relation between Water Occurrence and Laser Profile elevation (hereon WOLP), we derive
85 bathymetry maps using four (to five) steps: (a) acquiring the water occurrence from the global map by Pekel et al.
86 (2016), (b) extracting ICESat-2 data (ATL03 product) that coincide with the lake (defined as regions with >0%
87 water occurrence) in the water occurrence map (Figure 1a), (c) fitting a mathematical function describing the
88 relation between the two (Figure 1b), and (d) applying this function to translate water occurrence to lake-floor
89 elevation for the entire lake basin (Figure 1d). Where sub-basins exist, an additional step is needed between steps c
90 and d, in which we identify lake sub-basins from water occurrence, as detailed in Section 3 (e.g., Figure 1c). This
91 methodology provides a bathymetric map of lakes that were flooded to some extent between 1984 and 2015, with a
92 resolution of ~30 m.

93 To evaluate our methodology, we use available topographic data to demonstrate differences between our results and
94 available bathymetric (or topographic) maps. Where the SRTM is the best external source, we use cross-validation,
95 putting aside one ICESat-2 scan each time and validating the bathymetry based on all other scans. Owing to the high
96 accuracy of the ICESat-2 data, we demonstrate the small expected error using our methodology.

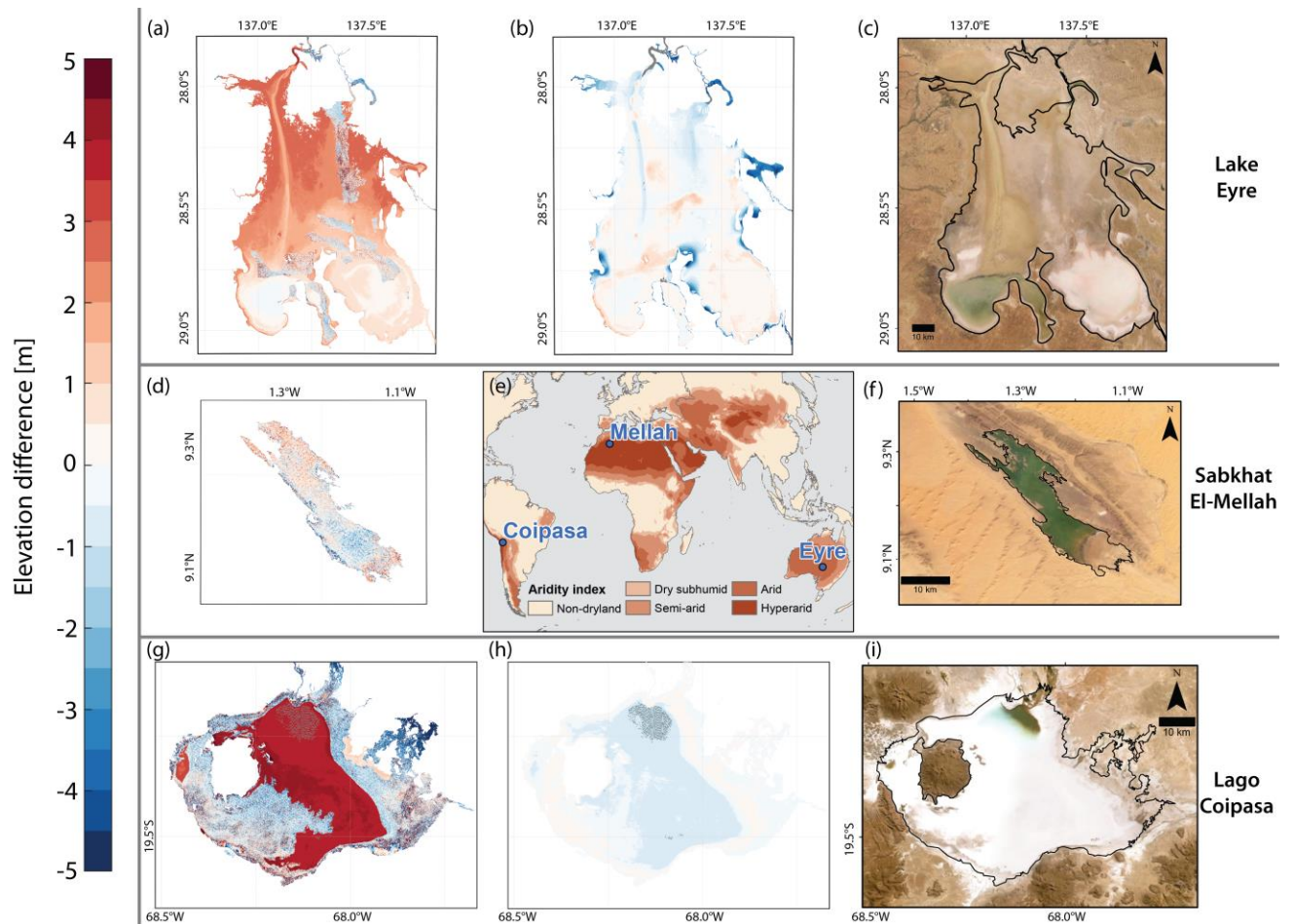


97

98 **Figure 1.** An example of bathymetry derivation in Lake Eyre North. (a) Water occurrence from
 99 Pekel et al. (2016) and ten ICESat-2 scans over the lake (labeled) used to derive elevations.
 100 Scans are colored by the 5 identified pseudo-watersheds (SI1). (b) The relation between water
 101 occurrence and elevation measurements from ICESat-2 scan #1 with a two-term gaussian fit and
 102 its 95% prediction boundaries. Colors represent latitude. (c) The same as in b, but for scan #3.
 103 The fit here is divided according to the watersheds. (d) Derived bathymetry map based on the
 104 methodology presented in Section 2. Gray dots represent regions in which water occurrence is
 105 greater than the highest occurrence overpassed by ICESat-2. B = Belt Bay. M = Madigan Gulf.
 106

107 3 Lake Eyre

108 Lake Eyre (Figure 2c, e) has a watershed covering almost 1% of the global land area ($>1.1 \times 10^6$ km²). It has a
 109 complex lake floor with a minimum elevation of -15.2 m relative to the Australian Height Datum (AHD) (Kotwicki
 110 and Isdale, 1991). The great flood of 1974 was utilized to perform bathymetric surveys over the lake, yielding a 0.5-
 111 m-contour-interval bathymetric map and detailing features >1 km² (Bye et al., 1978). Leon & Cohen (2012) (hereon
 112 LC12) combined data from this bathymetric map with SRTM data and ICESat-1 laser altimetry (with 170 m point
 113 spacing) to form the best bathymetric map of the lake that we are aware of. Because of its vast size, complex
 114 bathymetry, and a good reference map, we chose to apply our methodology over Lake Eyre. To have a continuous
 115 map, we only mapped Lake Eyre North (the larger and more frequently flooded part of the lake).
 116 To overcome complexity arising from the different relations of water occurrence and elevation in each of the sub-
 117 basins (Figure 1b), we divided Lake Eyre North into five sub-basins using the water occurrence map (Figure 1a;
 118 Supporting Information Figure 1 [S1]). This enabled identification of pseudo watersheds, similar to determining
 119 watersheds in a topographic map (SI1; Schwanghart and Scherler (2014)). We then performed steps b to d of our
 120 methodology, separately for each sub-basin (as exemplified in Figure 1c). If more than one ICESat-2 scan intersected a
 121 watershed, we used data from all available scans. To form a single map out of the different sub-basins, regions close
 122 to the pseudo water divide were assigned values using step c from all neighboring sub-basins, inversely weighted
 123 according to their distance from the divide (SI1).



124

125 **Figure 2.** Comparisons of WOLP bathymetries with SRTM data in Lake Eyre (a), Sabkhat El-
 126 Mellah (d), and Lago Coipasa (g). (b) Comparison of Lake Eyre bathymetry with the map of
 127 Leon & Cohen (2012). (e) Location map of the three lakes, and aridity index (UNEP, 1992) from
 128 the Climatic Research Unit of the University of East Anglia (New et al., 2002). True-color
 129 satellite imagery of the lakes from Esri\Digitalglobe, and maximum extent of water occurrence
 130 (in black) from Pekel et al. (2016) (c, f, i). (h) Difference between the “wet” and “dry”
 131 bathymetries of Lago Coipasa.
 132

133 We validated the WOLP bathymetry map (Figure 1d) against SRTM data and the LC12 bathymetry over the entire
 134 region (Table 1, Figures 2a, 2b), and against ICESat-2 scans over the measured profiles (Figure S2). The WOLP
 135 bathymetry lies within ± 0.5 m of LC12 elevations. For 74% of the region (90% is within ± 1 m), i.e., it lies within one
 136 elevation contour of Bye et al. (1978). Most of the remaining areas (deviating >1 m) are situated next to the lake
 137 margins, where the LC12 map is mostly based on SRTM data, which were acquired during a lake inundation
 138 interval, and are therefore not reliable over major parts of the lake (Leon and Cohen, 2012). In $\sim 83\%$ of the area
 139 SRTM data were replaced by a constant elevation value (-15 m AHD). The root mean square difference (RMSD) of
 140 the SRTM data versus the LC12 map is 1.77 m, and only 25% of the SRTM data are within ± 0.5 m of LC12,
 141 whereas the WOLP bathymetry has a RMSD of 0.52 m (Table 1). Moreover, the mean RMSD for each of the sub-
 142 basins using cross-validation of the different ICESat-2 scans is 0.21-0.57 m (Figure S3), indicating that the WOLP
 143 map error is even smaller than it seems when comparing it to the LC12 map.

144 Hypsometric curves emphasize differences between these analyzed bathymetries (Figure 3), and are important for
 145 water volume estimates (SI2). Whereas the SRTM wet area sharply increases above the minimum elevation, because
 146 of the constant (-15 m) elevation polygon, the WOLP and the LC12 wet area curves present a gradual increase with
 147 depth (Figure 3a). Accordingly, water volumes are lower by $\sim 75\%$ both in the WOLP and LC12 bathymetries

148 compared to the SRTM. Both the WOLP and the LC12 exhibit similar hypsometry in depths of <1 m (dissimilar to
 149 the SRTM). According to these maps, the southwestern sub-basin (Belt Bay) is the first to be filled (in accordance
 150 with MODIS imagery of floods, Supplementary movie 1 [SM1]). Differences between WOLP and LC12
 151 bathymetries increase above lake depths of 1 m, when the southeastern sub-basin (Madigan Gulf) fills according to
 152 WOLP bathymetry. In the LC12 map, the sill between the southern sub-basins is higher and therefore the flooded
 153 area increases only above water depth of 2 m. Large differences exist between WOLP and LC12 at the lake's
 154 margins; there, LC12 bathymetry rises ~5 m above the lake bottom (Figure 3a). These differences seem to be related
 155 to the SRTM-dependent mapping of the lake margins in LC12. At a depth of 3.1 m, the WOLP flooded area reaches
 156 its maximum extent, featuring an area of $6.1 \times 10^3 \text{ km}^2$ and a volume of 8.9 km^3 , ~33% higher than the respective
 157 area and volume calculated based on the LC12 map (Figure 3a). Nevertheless, it is important to note that WOLP
 158 bathymetry represents only regions that were flooded between 1984 and 2015, and that the largest flood in recent
 159 history occurred in the 1970's. Therefore higher shorelines, as in LC12 or Cohen et al. (2018), could not be mapped
 160 with WOLP.

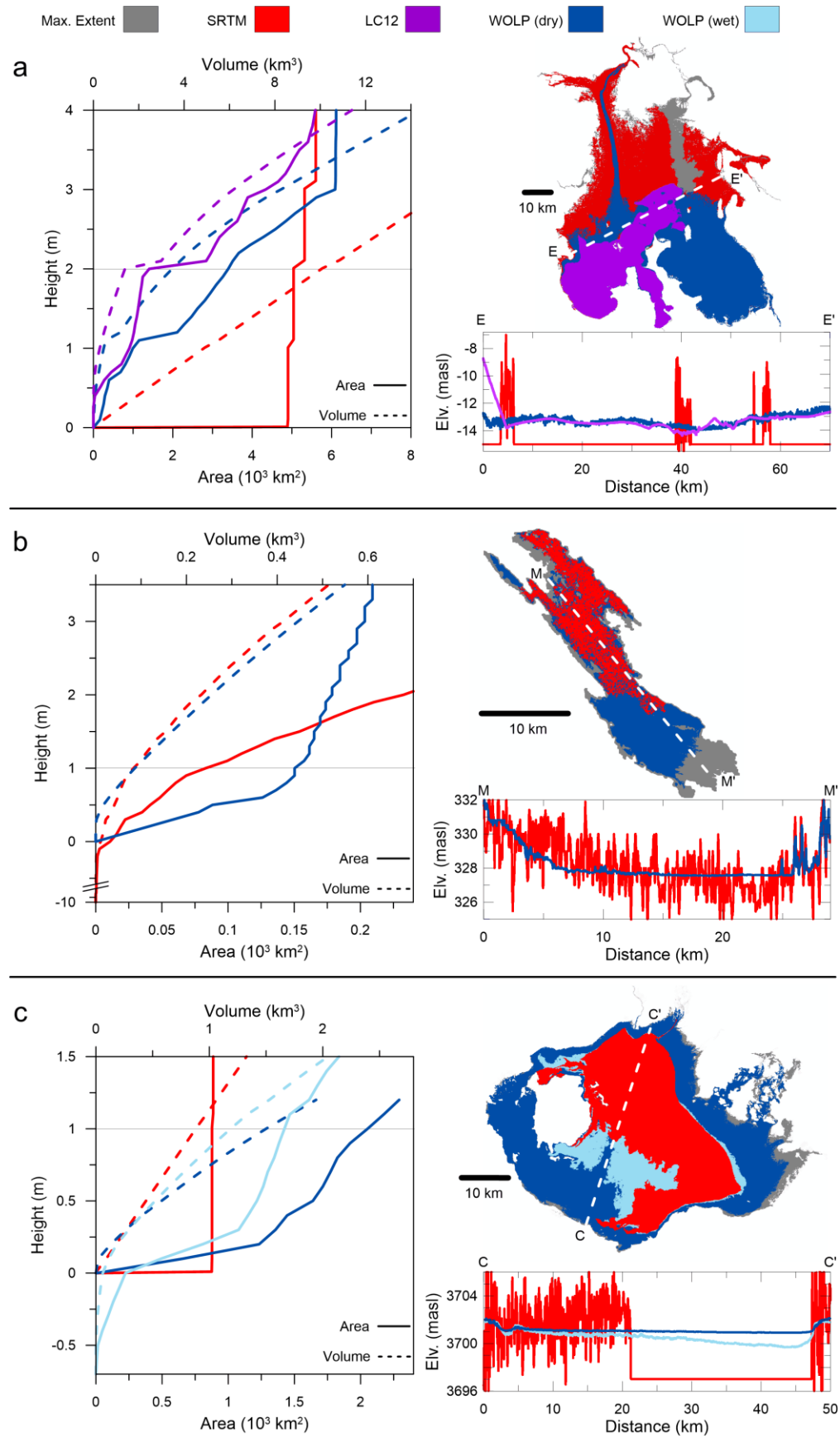
161 **Table 1.** *Validation results across the lakes*

Lake	Validated map	Reference	Regional / Profile validation	RMSD [m]	Lake depth [m]
Lake Eyre	SRTM	LC12	Regional	1.77	3.2 (WOLP) [§] , 4.1 (LC12) [§]
	WOLP (this study)	LC12	Regional	0.52	
	SRTM	ICESat-2	Profile	0.95-2.30*	
	LC12	ICESat-2	Profile	0.20-0.69*	
	WOLP	ICESat-2	Profile, cross-validation	0.21-0.57*	
Sabkhat El-Mellah	SRTM	ICESat-2	Profile	2.04 [#]	5.0 (WOLP) [§]
	WOLP	ICESat-2	Profile, cross-validation	0.32 [#]	
Lago Coipasa	SRTM	ICESat-2	Profile	2.84 [#]	1.2 (WOLP: "dry") [§]
	WOLP ("dry")	ICESat-2	Profile, cross-validation	0.28 [#]	
	WOLP ("wet")	WOLP ("dry")	Regional	0.39	2.2 (WOLP: "wet") [§]
	WOLP ("wet")	ICESat-2	Profile, cross-validation	0.47 [#]	

162 *Range denotes the average RMSD for each sub-basin, averaged between the different ICESat-2 profiles in it.

163 [#]Average among the different ICESat-2 profiles.

164 [§]Estimated (see SI2).



166 **Figure 3.** Hypsometric curves, extent maps and cross-sections for Lake Eyre (a), Sabkhat El-
 167 Mellah (b), and Lago Coipasa (c). The maps show filling extent at heights (denoted by a gray
 168 line on the hypsometric curves) that exert major differences between bathymetries. Details of the
 169 preparation of the hypsometries are in SI2.
 170

171 **4 Application for non-mapped and inundated lakes**

172 Sabkhat El-Mellah is a small, northwestern Sahara ephemeral lake ($\sim 170 \text{ km}^2$) (Figure 2e, f). It is fed in the High
 173 Atlas Mountains and is flooded only once every few years (Mabbutt, 1977). There is no bathymetric map of this lake
 174 that we are aware of. A comparison of the WOLP bathymetry (Figure S4) to the SRTM data (Figures 2d, S5)
 175 indicates generally a similar pattern (location of the deepest part of the lake and its margins, large scale slopes, etc.).
 176 However, variations of the SRTM data over Sabkhat El-Mellah are approximately $\pm 2 \text{ m}$ (Figures 3b, S5), while lake
 177 depth is $\sim 5 \text{ m}$, yielding an uncharacteristic discontinuous and rough lake floor (e.g., Quade et al., 2018). The mean
 178 cross-validation RMSD of WOLP bathymetry is much lower (0.32 m; Table 1, Figure S6). The WOLP map exhibits
 179 a much higher flooded area in comparison with the SRTM data (Figure 3b). E.g., at a 1 m lake depth, the WOLP
 180 lake area is $0.15 \times 10^3 \text{ km}^2$ versus $0.08 \times 10^3 \text{ km}^2$ according to SRTM data.

181 The same methodology was applied over Lago Coipasa (or Salar de Coipasa; surface area up to 2400 km^2), which is
 182 a high altitude (3660 m), shallow saline lake, occasionally filled with water (Placzek et al., 2006) (Figure 2e, i).
 183 However, during February 2019, the lake was flooded (SM2), thus, ICESat-2 scans taken afterward exhibit both the
 184 water surface and the lake floor in its inundated region.

185 Recent studies highlight the ability of ICESat-2 scans to penetrate water and yield bathymetric profiles (Forfinski-
 186 Sarkozi and Parrish, 2016; Ma et al., 2019; Parrish et al., 2019). Therefore, we derived two different bathymetric
 187 maps of Lago Coipasa, one using all available “dry” scans (i.e., before February 2019; Figure S7), and the other
 188 (Figure S8) using only post-flood scans (“wet” scans), manually omitting the ICESat-2’s water surface readings
 189 (SI3). The difference between the “dry” bathymetry and the SRTM data, and the difference between the “dry” and
 190 “wet” maps are shown in Figures 2g and 2h, respectively. Given the difficulty in determining water density, we did
 191 not correct the effect of the changing refraction coefficient between water and air on underwater elevation
 192 measurements. However, to avoid location errors, we used only nadir data, which are expected to have the least
 193 spatial error. The expected vertical error where water depth is $\sim 0.7 \text{ m}$ (SI3), as in this 2019 flood, is $< 0.18 \text{ m}$
 194 (Parrish et al., 2019) or even less (as shown in Ma et al., 2019).

195 Similar to Lake Eyre, the WOLP-SRTM difference map (Figure 2g) illustrates that Lago Coipasa was inundated
 196 during the SRTM scan, and the wet part of the scan was replaced with a fixed elevation value. The SRTM data over
 197 the lake area varies within $\sim \pm 5 \text{ m}$ (RMSD=2.84 m; Figures 3c and S9), meaning that over a $\sim 1.5 \text{ m}$ deep lake, such
 198 as Lago Coipasa, SRTM-based water volume calculations for all practical matters are absurd. In contrast, both the
 199 “dry” and the “wet” WOLP bathymetries yield a much smaller mean cross-validation RMSD value (0.28 m and 0.47
 200 m, respectively; Table 1, Figures S10, S11).

201 The fixed-elevation polygon in the SRTM data for Lago Coipasa is bounded by high ($> 2 \text{ m}$) artificial walls. This is
 202 exhibited in the hypsometry by a sharp increase and then a fixed wetted area of $0.87 \times 10^3 \text{ km}^2$ (Figure 3c). In lake
 203 depths of $< 1 \text{ m}$, the “dry” bathymetry presents a detailed gradual increase in lake area and volume, filling most of
 204 the maximum lake extent. The “wet” WOLP area at 1 m depth is smaller than the “dry” area due to a 1.3 m deeper
 205 lake bottom in the “wet” bathymetry (Figure 3c; SI2). Both the “dry” and “wet” scans did not cross the northernmost
 206 part of the lake, which is characterized by the highest water occurrence (and presumably deepest water column). For
 207 this reason, we stress that future crossing of ICESat-2 over this specific region of the lake could improve its
 208 bathymetry.

209 Compared with the “dry” bathymetry, 58% of the “wet” lake area lies within $\pm 0.5 \text{ m}$ of the “dry” bathymetry
 210 (RMSD = 0.39 m). Thus, relying on the “dry” bathymetric map, which seems reasonable in light of the results
 211 shown for Lake Eyre, we suggest that even when using only the “wet” scans, the WOLP bathymetry yields better
 212 results than the currently available global product (SRTM). This leads us to propose the usage of the methodology
 213 presented here for any of the world’s shallow desert lakes.

214 **5 Discussion**

215 The largest source of uncertainty in the WOLP bathymetry stems from the selected fitting equation between water
 216 occurrence and elevation (step c). However, this selection affects mainly the extremities of data, i.e., the
 217 extrapolation of elevation to values that were not observed by the ICESat-2 (areas with gray dots in Figures 1c, S4,

218 S7, S8). Thus, in cases where ICESat-2 data covers the water frequency extremities, WOLP bathymetry is accurate,
219 as demonstrated by the cross-validation results. Large enough lakes should be covered by at least a few ICESat-2
220 scans (e.g., Figure 1a) and therefore, scans are expected to cover a wide range of water occurrences. This wide range
221 can yield an accurate bathymetry for almost all of the lake extent.

222 Laser altimetry errors, estimated to be ~ 0.3 m for a single photon return, and much lower (0.05-0.07 m) for an
223 average of neighboring photon returns (Jasinski et al., 2016), are not expected to impact our results significantly. A
224 larger uncertainty lies between points that have a similar water occurrence but different elevation, as is the case if
225 there are small and local topographic minima. Using more scans may decrease the variations, although some of them
226 may be intrinsic, e.g., where transmission-losses or springs are common. Water occurrence minima can be too small
227 to be identified as a different sub-basin. Thus, our method is limited to sub-basins that are large enough to be
228 resolved with ICESat-2, as in Lake Eyre (Figure 1, S11). In deriving the Lake Eyre bathymetry, we used at least four
229 scans for each sub-basin, yielding an error of only 0.2-0.6 m (Table 1, Figure S3).

230 Another limitation to our methodology comes from the maximum water penetration of the ICESat-2 laser. This
231 limits the ability to derive bathymetry in lakes that have a water depth of tens of meters or more. In such
232 circumstances, a partial bathymetry could still be derived for the outskirts of the lakes using our methodology, or as
233 presented in Li et al. (2019) or in Ma et al. (2019) for the shoulders of Lake Mead. However, we focus here on
234 shallow desert lakes, in which, by definition, this is not a major obstacle.

235 Sediment deposition could also increase the uncertainty of the derived bathymetry. Here, we use satellite imaging
236 water occurrence from >30 -yr period (Pekel et al., 2016), implying that if the lake floor was altered during this time
237 interval, present-day ICESat-2 scans can yield only an averaged bathymetry of this period. However, newer global
238 water occurrence datasets could emerge in the near future, enabling both derivation of newer bathymetries, and
239 higher resolution maps (e.g., 10-20 m pixels from Sentinel-2).

240 Apart from these limitations, taking a long series of satellite imagery extends a great opportunity. If only specific
241 dates are used to identify isobaths (or shorelines), the error propagates to the bathymetric map. Using statistics based
242 on many years, single image errors diminish. Such errors include water piling-up on one side of the lake due to
243 winds (Arsen et al., 2013), misclassification of water boundaries or crossing isobaths (Long et al., 2019), and
244 specific date imaging having only partial coverage of a lake, because of imaging geometry or cloud obscuration.
245 Moreover, the use of specific date imagery requires a spatial interpolation between isobaths, thus concealing small
246 features in between isobaths.

247 Out of the three lakes analyzed above, Lake Eyre is probably the most closely monitored, yet the nearest river gauge
248 is situated many hundreds of kilometers upstream. Therefore, there is no accurate in-situ data for water input
249 volumes. ICESat-2's high spatial resolution (~ 70 cm) combined with high-resolution water occurrence map (e.g., 30
250 m in the map of Pekel et al., 2016) yields an accurate, high-resolution bathymetry, even over flooded or complex
251 desert lakes. Such maps could help in determining the water discharge into remote desert lakes and their evaporative
252 losses, providing much-needed data in remote areas, serving as a basis for mass and energy balance calculations
253 over such lakes, and for water management strategies.

254 **6 Conclusions**

255 Using a new methodology which links long-term water occurrence and accurate height measurements, each
256 independently derived from satellite remote-sensing, we mapped the bathymetry of three shallow lakes in drylands
257 across the globe. We verified the bathymetries using a previous bathymetric map, SRTM data, and through cross-
258 validation. This easy-to-implement methodology yields a high-resolution bathymetry of shallow desert lakes that
259 were flooded sometime during 1984-2015, using globally available datasets.

- 260 - As an example of a complex shallow lake system, we used Lake Eyre, consisting of multiple sub-basins.
261 Despite its complexity, verification versus the best available DEM showed that the methodology is
262 successful, as long as each sub-basin is covered by an elevation measurement scan.
- 263 - The methodology was also applied to two lakes with no previous bathymetry maps, one in the Sahara
264 (Sabkhat El-Mellah) and the other in the Altiplano (Lago Coipasa). Results proved low cross-validation
265 RMSD values (~ 0.3 m) compared with the SRTM data (~ 2.5 m).
- 266 - Applying the methodology in Lago Coipasa separately to “dry” and to “wet” ICESat-2 scans, relying on
267 laser penetrability, we showed that bathymetry can even be produced during lake inundation.

268 The presented methodology can be applied to a large portion of the shallow lakes around the globe. It enables
269 mapping of inundated lakes (a major obstacle for widely used methods), small lakes, and large and complex lake
270 systems.

271 **Acknowledgments and Data**

272 This research was supported by ISF grant 946/18 and NSFC-ISF grant 2487/17 to YE. Water occurrence data (Pekel
273 et al., 2016) were obtained from <https://global-surface-water.appspot.com>, using Google Earth Engine
274 (<https://earthengine.google.com/>). ICESat-2 ATL03 data were obtained from <https://openaltimetry.org/data/icesat2/>:
275 Neumann, T. A., A. Brenner, D. Hancock, J. Robbins, J. Saba, K. Harbeck, and A. Gibbons. 2019. ATLAS/ICESat-
276 2 L2A Global Geolocated Photon Data, V1. [ATL03]. Boulder, Colorado USA. NSIDC: National Snow and Ice
277 Data Center. doi: <https://doi.org/10.5067/ATLAS/ATL03.001>. [Dec 2019]. The authors declare no conflict of
278 interests.

279 **References**

- 280 Arsen, A., Crétaux, J. F., Berge-Nguyen, M. and del Rio, R. A.: Remote sensing-derived bathymetry of Lake Poopó,
281 *Remote Sens.*, 6(1), 407–420, doi:10.3390/rs6010407, 2013.
- 282 Berry, P. A. M., Garlick, J. D. and Smith, R. G.: Near-global validation of the SRTM DEM using satellite radar
283 altimetry, *Remote Sens. Environ.*, 106(1), 17–27, doi:10.1016/j.rse.2006.07.011, 2007.
- 284 Brenner, A. C., DiMarzio, J. P. and Zwally, H. J.: Precision and accuracy of satellite radar and laser altimeter data
285 over the continental ice sheets, *IEEE Trans. Geosci. Remote Sens.*, 45(2), 321–331,
286 doi:10.1109/TGRS.2006.887172, 2007.
- 287 Brunt, K. M., Neumann, T. A. and Smith, B. E.: Assessment of ICESat-2 Ice Sheet Surface Heights, Based on
288 Comparisons Over the Interior of the Antarctic Ice Sheet, *Geophys. Res. Lett.*, 46, 13072–13078,
289 doi:10.1029/2019GL084886, 2019.
- 290 Bye, J. A. T., Dillon, P. J., Vandenberg, J. C. and Will, G. D.: Bathymetry of Lake Eyre, *Trans. R. Soc. South Aust.*,
291 102(1), 85–89, doi:10.1080/00359196009519029, 1978.
- 292 Cohen, T. J., Jansen, J. D., Gliganic, L. A., Larsen, J. R., Nanson, G. C., May, J. H., Jones, B. G. and Price, D. M.:
293 Hydrological transformation coincided with megafaunal extinction in central Australia, *Geology*, 43(3), 195–198,
294 doi:10.1130/G36346.1, 2015.
- 295 Cohen, T. J., Meyer, M. C. and May, J. H.: Identifying extreme pluvials in the last millennia using optical dating of
296 single grains of quartz from shorelines on Australia’s largest lake, *Holocene*, 28(1), 150–165,
297 doi:10.1177/0959683617715700, 2018.
- 298 Crétaux, J. F., Abarca-del-Río, R., Bergé-Nguyen, M., Arsen, A., Drolon, V., Clos, G. and Maisongrande, P.: Lake
299 Volume Monitoring from Space, *Surv. Geophys.*, 37(2), 269–305, doi:10.1007/s10712-016-9362-6, 2016.
- 300 D’Odorico, P. and Porporato, A.: *Dryland ecohydrology.*, 2006.
- 301 Enzel, Y. and Wells, S. G.: Extracting Holocene paleohydrology and paleoclimatology information from modern
302 extreme flood events: An example from southern California, *Geomorphology*, 19(3–4), 203–226,
303 doi:10.1016/s0169-555x(97)00015-9, 1997.
- 304 Feng, L., Hu, C., Chen, X., Li, R., Tian, L. and Murch, B.: MODIS observations of the bottom topography and its
305 inter-annual variability of Poyang Lake, *Remote Sens. Environ.*, 115(10), 2729–2741,
306 doi:10.1016/j.rse.2011.06.013, 2011.
- 307 Forfinski-Sarkozi, N. A. and Parrish, C. E.: Analysis of MABEL bathymetry in Keweenaw Bay and implications for
308 ICESat-2 ATLAS, *Remote Sens.*, 8(9), doi:10.3390/rs8090772, 2016.
- 309 Gao, H.: Satellite remote sensing of large lakes and reservoirs: from elevation and area to storage, *Wiley Interdiscip.*
310 *Rev. Water*, 2(2), 147–157, doi:10.1002/wat2.1065, 2015.
- 311 Jasinski, M. F., Stoll, J. D., Cook, W. B., Ondrusek, M., Stengel, E. and Brunt, K.: Inland and Near-Shore Water
312 Profiles Derived from the High-Altitude Multiple Altimeter Beam Experimental Lidar (MABEL), *J. Coast. Res.*, 76,
313 44–55, doi:10.2112/si76-005, 2016.
- 314 Jawak, S. D., Vadlamani, S. S. and Luis, A. J.: A Synoptic Review on Deriving Bathymetry Information Using
315 Remote Sensing Technologies: Models, Methods and Comparisons, *Adv. Remote Sens.*, 04(02), 147–162,
316 doi:10.4236/ars.2015.42013, 2015.
- 317 Kotwicki, V. and Isdale, P.: Hydrology of Lake Eyre, Australia: El Niño link, *Palaeogeogr. Palaeoclimatol.*
318 *Palaeoecol.*, 84(1–4), 87–98, doi:10.1016/0031-0182(91)90037-R, 1991.
- 319 Leon, J. X. and Cohen, T. J.: An improved bathymetric model for the modern and palaeo Lake Eyre,
320 *Geomorphology*, 173–174, 69–79, doi:10.1016/j.geomorph.2012.05.029, 2012.
- 321 Li, Y., Gao, H., Jasinski, M. F., Zhang, S. and Stoll, J. D.: Deriving High-Resolution Reservoir Bathymetry From
322 ICESat-2 Prototype Photon-Counting Lidar and Landsat Imagery, *IEEE Trans. Geosci. Remote Sens.*, PP(June), 1–
323 11, doi:10.1109/tgrs.2019.2917012, 2019.

- 324 Long, Y., Yan, S., Jiang, C., Wu, C., Tang, R. and Hu, S.: Inversion of Lake Bathymetry through Integrating Multi-
325 Temporal Landsat and ICESat Imagery, *Sensors*, 19(13), 2896, doi:10.3390/s19132896, 2019.
- 326 Ma, Y., Xu, N., Sun, J., Wang, X. H., Yang, F. and Li, S.: Estimating water levels and volumes of lakes dated back
327 to the 1980s using Landsat imagery and photon-counting lidar datasets, *Remote Sens. Environ.*, 232(July), 111287,
328 doi:10.1016/j.rse.2019.111287, 2019.
- 329 Mabbutt, J. A.: *Desert landforms*, Second pri., The MIT Press, Cambridge, Massachusetts, USA., 1977.
- 330 Markus, T., Neumann, T., Martino, A., Abdalati, W., Brunt, K., Csatho, B., Farrell, S., Fricker, H., Gardner, A.,
331 Harding, D., Jasinski, M., Kwok, R., Magruder, L., Lubin, D., Luthcke, S., Morison, J., Nelson, R.,
332 Neuenschwander, A., Palm, S., Popescu, S., Shum, C. K., Schutz, B. E., Smith, B., Yang, Y. and Zwally, J.: The Ice,
333 Cloud, and land Elevation Satellite-2 (ICESat-2): Science requirements, concept, and implementation, *Remote Sens.*
334 *Environ.*, 190, 260–273, doi:10.1016/j.rse.2016.12.029, 2017.
- 335 de Martonne, E.: Regions of Interior-Basin Drainage, *Geogr. Rev.*, 17(3), 397–414, 1927.
- 336 New, M., Lister, D., Hulme, M. and Makin, I.: A high-resolution data set of surface climate over global land areas,
337 *Clim. Res.*, 21(1), 1–25, doi:10.3354/cr021001, 2002.
- 338 Nicholson, S. E.: *Dryland climatology*, Cambridge University Press, New York., 2011.
- 339 Noy-Meir, I.: Desert Ecosystems: Environment and Producers, *Annu. Rev. Ecol. Syst.*, 4, 25–51, 1973.
- 340 Parrish, C. E., Magruder, L. A., Neuenschwander, A. L., Forfinski-Sarkozi, N., Alonzo, M. and Jasinski, M.:
341 Validation of ICESat-2 ATLAS Bathymetry and Analysis of ATLAS’s Bathymetric Mapping Performance, *Remote*
342 *Sens.*, 11(14), 1634, doi:10.3390/rs11141634, 2019.
- 343 Pekel, J. F., Cottam, A., Gorelick, N. and Belward, A. S.: High-resolution mapping of global surface water and its
344 long-term changes, *Nature*, 540(7633), 418–422, doi:10.1038/nature20584, 2016.
- 345 Placzek, C., Quade, J. and Patchett, P. J.: Geochronology and stratigraphy of late Pleistocene lake cycles on the
346 southern Bolivian Altiplano: Implications for causes of tropical climate change, *Bull. Geol. Soc. Am.*, 118(5–6),
347 515–532, doi:10.1130/B25770.1, 2006.
- 348 Quade, J., Dente, E., Armon, M., Ben Dor, Y., Morin, E., Adam, O. and Enzel, Y.: Megalakes in the Sahara? A
349 Review, *Quat. Res. (United States)*, 90(2), 253–275, doi:10.1017/qua.2018.46, 2018.
- 350 Schwanghart, W. and Scherler, D.: Short Communication: TopoToolbox 2 - MATLAB-based software for
351 topographic analysis and modeling in Earth surface sciences, *Earth Surf. Dyn.*, 2(1), 1–7, doi:10.5194/esurf-2-1-
352 2014, 2014.
- 353 Sun, F. and Ma, R.: Hydrologic changes of Aral Sea: A reveal by the combination of radar altimeter data and optical
354 images, *Ann. GIS*, 25(3), 247–261, doi:10.1080/19475683.2019.1626909, 2019.
- 355 UNEP: *World atlas of desertification*, London : Edward Arnold, London., 1992.
- 356